nature cell biology

Phagocytic activity of neuronal progenitors regulates adult neurogenesis

Zhenjie Lu[1], Michael R. Elliott[2], Yubo Chen[1,5], James T. Walsh[1], Alexander L. Klibanov[3], Kodi S. Ravichandran[2,4,6] and Jonathan Kipnis[1,6]

Whereas thousands of new neurons are generated daily during adult life, only a fraction of them survive and become part of neural circuits; the rest die, and their corpses are presumably cleared by resident phagocytes. How the dying neurons are removed and how such clearance influences neurogenesis are not well understood. Here, we identify an unexpected phagocytic role for the doublecortin (DCX)-positive neuronal progenitor cells during adult neurogenesis. Our *in vivo* and *ex vivo* studies demonstrate that DCX$^+$ cells comprise a significant phagocytic population within the neurogenic zones. Intracellular engulfment protein ELMO1, which promotes Rac activation downstream of phagocytic receptors, was required for phagocytosis by DCX$^+$ cells. Disruption of engulfment *in vivo* genetically (in *Elmo1*-null mice) or pharmacologically (in wild-type mice) led to reduced uptake by DCX$^+$ cells, accumulation of apoptotic nuclei in the neurogenic niches and impaired neurogenesis. Collectively, these findings indicate a paradigm wherein DCX$^+$ neuronal precursors also serve as phagocytes, and that their phagocytic activity critically contributes to neurogenesis in the adult brain.

The subventricular zone (SVZ) of the lateral ventricles and the subgranular zone (SGZ) of the hippocampal dentate gyrus represent two active neurogenic niches in the adult brain[1–6]. These neurogenic areas contain neural progenitor cells (NPCs) capable of generating new neurons and glial cells (astrocytes and oligodendrocytes). Thousands of new neurons are generated daily[7–11], although only a fraction of the doublecortin-positive (DCX$^+$) neuronal progenitors survive[12–16]. The process by which the dying DCX$^+$ cells are removed, and how such removal impacts neurogenesis, are not known. Excess cells in many tissues die by apoptosis; the exposure of phosphatidylserine (PtdSer) on dying cells is a key 'eat-me' signal facilitating the recognition and phagocytic removal by resident phagocytes[17–19]. PtdSer on apoptotic cells can either be recognized directly (via receptors such as BAI1, TIM-4 and Stabilin-2), or indirectly through soluble bridging molecules and in turn recognized by other phagocytic receptors (such as Mer or integrin $\alpha_v\beta_3$; refs 17–19).

To better define the phagocytic process in the neurogenic niches, we injected fluorescently labelled PtdSer-containing liposomes (Supplementary Fig. S1a) into the SVZ of 8–12-week-old wild-type mice and examined the presence of the phagocytosed liposomes inside cells within the niche (Supplementary Fig. S1b). We initially focused on glial fibrillary acidic protein (GFAP)-expressing cells (niche astrocytes and astrocyte stem cells[20–23]), because glial cells in mammals[24,25] and other organisms[26,27] can play major phagocytic roles during development. Surprisingly, many of the ingested liposomes were found within DCX$^+$ neuronal precursor cells in the SVZ (Fig. 1a) and the SGZ (Supplementary Fig. S1c). Among liposome-engulfing cells in the SVZ, $56 \pm 6\%$ were DCX$^+$ cells, whereas $44 \pm 6\%$ were DCX$^-$ cells within the 200 μm range of the injection site. Mice injected with control phosphatidylcholine (PtdCho)-containing liposomes showed poor ingestion by DCX$^+$ cells (Fig. 1c). Injection of ultraviolet-irradiated (apoptotic) fluorescently labelled NPCs also showed that DCX cells are phagocytic, and that they can ingest apoptotic NPCs (Fig. 1b). However, owing to relatively poor diffusion of NPCs when compared with liposomes, only $12 \pm 2\%$ of DCX$^+$ cells engulfed ultraviolet-irradiated progenitors within the 200 μm range of the injection site.

It has been previously shown by several groups that injection of annexin V (a protein that binds PtdSer on apoptotic cells and inhibits engulfment) intravenously can reach the central nervous system (CNS) (refs 28,29) and other organs[30] (Supplementary Fig. S2a). Intravenous injection of annexin V before intracranial injection of liposomes blocked the uptake of PtdSer liposomes by DCX$^+$ cells *in vivo* (Fig. 1d). These data indicate that DCX$^+$ cells are phagocytic cells within the neurogenic niches and that they use a PtdSer-dependent recognition for uptake.

[1]Department of Neuroscience, University of Virginia, Charlottesville, Virginia 22901, USA. [2]Beirne B. Carter Center for Immunology Research, University of Virginia, Charlottesville, Virginia 22901, USA. [3]Cardiovascular Research Center, University of Virginia, Charlottesville, Virginia 22901, USA. [4]Center for Cell Clearance, University of Virginia, Charlottesville, Virginia 22901, USA. [5]Present address: Key Laboratory for NeuroInformation of Ministry of Education, University of Electonic Science and Technology of China, ChengDu, 610054, China.
[6]Correspondence should be addressed to K.S.R. or J.K. (e-mail: Ravi@virginia.edu or Kipnis@virginia.edu)

Received 19 November 2010; accepted 15 June 2011; published online 31 July 2011; DOI: 10.1038/ncb2299

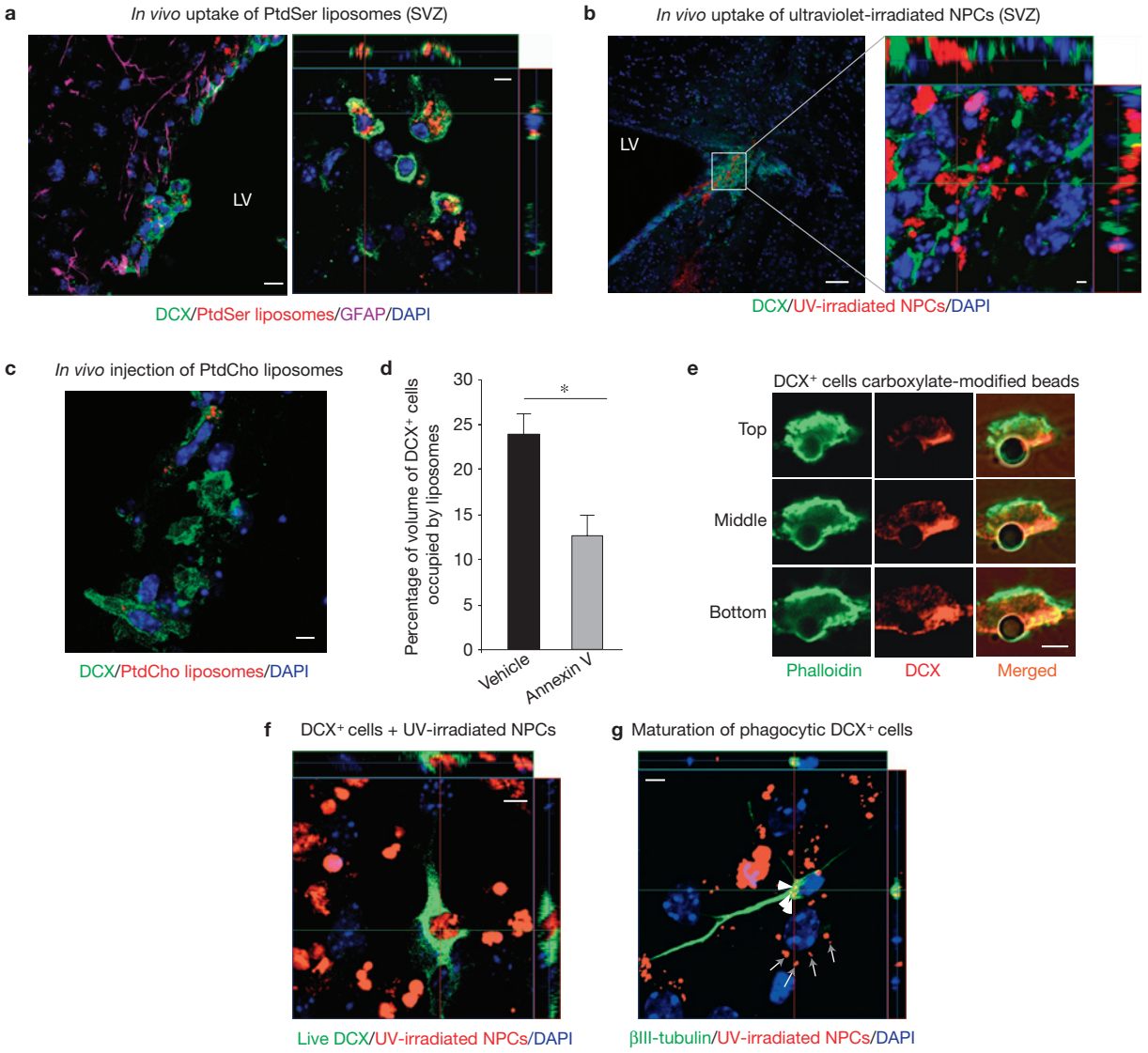

Figure 1 DCX-expressing neuronal progenitor cells exhibit phagocytic activity *in vivo* and *ex vivo*. (**a**) Wild-type mice (LV, lateral ventricle) intracranially injected with fluorescent PtdSer liposomes examined immunohistochemically in the SVZ for DCX^+ and $GFAP^+$ cells with phagocytosed liposomes. DAPI, 4,6-diamidino-2-phenylindole. Representative confocal micrographs are shown ($n > 10$ fields analysed per experiment; five independent experiments carried out). Scale bar, 10 μm (5 μm in inset). (**b**) Wild-type mice intracranially injected with fluorescently labelled ultraviolet (UV)-irradiated NPCs examined immunohistochemically in the SVZ for DCX^+ cells with phagocytosed cells. A representative micrograph is shown in orthogonal projections of confocal *z* stacks ($n > 12$ fields analysed per experiment; three independent experiments carried out). Scale bar, 50 μm (2 μm in inset). (**c**) Wild-type mice intracranially injected with fluorescent PtdCho liposomes exhibit poor engulfment by DCX^+ cells in the SVZ ($n > 10$ fields analysed per experiment; three independent experiments carried out). Scale bar, 5 μm. (**d**) Wild-type mice injected intravenously with annexin V before and immediately after intracranial injection with fluorescent PtdSer liposomes. Brain tissue examined immunohistochemically for DCX^+ and $GFAP^+$ cells containing liposomes in the SVZ. The bar graph represents a quantification of the volume of DCX^+ cells containing PtdSer liposomes (mean ± s.e.m.). Student's *t*-test statistical analysis was carried out for $n = 4$ mice in each group with at least five slices analysed for each mouse ($^*P < 0.05$). (**e**) Representative confocal microscopy images (with $n > 30$ cells analysed), demonstrating the formation of the phagocytic cup (phalloidin staining) in DCX^+ cells around the carboxylate-modified 3 μm beads (simplified apoptotic targets), are shown in top, middle and bottom planes. Scale bar, 3 μm. (**f**) Representative confocal microscopy images of phagocytosis by a newly differentiated neuron showing orthogonal projections of confocal *z* stacks ($n > 20$ fields analysed per experiment; seven independent experiments carried out). Scale bar, 5 μm. (**g**) Newly differentiated NPC cultures were fed with ultraviolet-irradiated NPCs *ex vivo* and washed after 6 h. Cells were analysed after a further seven days of differentiation. Representative confocal microscopy orthogonal views of maturated neurons are shown. White arrowheads point to remnants of phagocytosed cells in neurons and grey arrows those in other cells ($n > 20$ fields analysed per experiment; four independent experiments carried out). Scale bar, 5 μm.

Although microglial cells are the resident myeloid cells of the CNS with known phagocytic capacity[31–33], activated microglia are hardly detectable in non-inflamed CNS, with only very few microglia phagocytosing the injected NPCs (Supplementary Fig. S2b).

To better define the phagocytic capacity of DCX^+ cells, differentiated neurospheres from SVZ cells were incubated with simplified targets that mimic certain properties of apoptotic cells (negatively charged carboxylate-modified 3 μm beads, whose uptake is blocked by

annexin V; refs 34,35). The DCX$^+$ cells engulfed these targets, showing the phagocytic cup and the actin ring around the target (Fig. 1e). DCX$^+$ neuronal precursors also efficiently engulfed apoptotic NPCs *in vitro* (Fig. 1f).

To determine whether early neuronal progenitors (DCX$^+$) engulfing the dead neural precursor cells could differentiate into neurons, fluorescently labelled irradiated NPCs were added to newly differentiated dissociated neurospheres (24 h in culture) for 6 h. After washing and further 7 days, the cultures were examined for expression of a later neuronal differentiation marker (βIII-tubulin). The remnants of the engulfed fluorescently labelled particles were evident in βIII-tubulin$^+$ cells, indicating that DCX$^+$ precursors that have engulfed other NPCs can differentiate into βIII-tubulin$^+$ neurons (Fig. 1g). Incubation of differentiating NPC cultures with irradiated progenitors had no detectable effect on neuronal differentiation under these conditions ($19\pm4\%$ versus $17\pm4\%$; neuronal differentiation ±s.e.m. in control media or after treatment with irradiated progenitor cells, respectively). However, addition of a high burden of the dead progenitors resulted in accelerated death of the NPC cultures, indicating that too many dead cells create an unfavourable environment.

To address the physiological role for engulfment by DCX$^+$ cells within neurogenic areas, we tested the effect of inhibiting phagocytosis on adult neurogenesis. After intravenous injection of annexin V to inhibit apoptotic cell clearance, we assessed neurogenesis (schematic representation in Fig. 2a). First, compared with the saline, annexin V treatment led to substantial accumulation of TdT-mediated dUTP nick end labelling (TUNEL)-positive nuclei in the SGZ and SVZ (Fig. 2b and Supplementary Fig. S3). Second, we observed a striking reduction in neuronal differentiation (bromodeoxyuridine (BrdU)$^+$DCX$^+$ cells) and survival (BrdU$^+$NeuN$^+$ cells) in the SGZ (Fig. 2c,d) and in neuronal differentiation (DCX$^+$ cells) in the SVZ (Fig. 2e). Importantly, the overall number of proliferating cells (BrdU$^+$) in the SGZ did not change on annexin V treatment. This indicates that, whereas the numbers of neuronal progenitors (DCX$^+$ cells) are reduced, there might be an increase in the numbers of non-differentiated NPCs. These data imply that death and clearance of neurons in the neurogenic niches is an ongoing process, and that interference with phagocytic clearance significantly impacts neurogenesis.

We next addressed the molecular mechanism(s) contributing to phagocytosis by DCX$^+$ cells. ELMO1 is a cytoplasmic evolutionarily conserved protein important for the clearance of dying cells[35]. ELMO1 binds to the cytoplasmic tail of the membrane receptor brain angiogenesis inhibitor 1 (Bai1) and activates the small GTPase Rac1, and thereby promotes cytoskeletal rearrangements to engulf apoptotic cells[34]. Loss of ELMO1, or mutations in ELMO1, can severely impair engulfment both *in vitro*[35] and *in vivo*[35,36].

To address a possible role for ELMO1 in phagocytosis by DCX$^+$ neuronal progenitor cells, we first examined ELMO1 expression in DCX$^+$ cells. Primary hippocampal neurons were cultured for 2 or 6 days *in vitro* and examined for ELMO1 expression. Whereas high levels of ELMO1 were detected in neurons after 2 days, ELMO1 levels dropped significantly after 6 days in culture (Fig. 3a). In contrast, the level of ELMO2 was not altered under these conditions (Fig. 3b). When the DCX$^+$ cells were fed with apoptotic targets, the phagocytic capacity of DCX$^+$ cells after 2 days in culture was significantly higher than after 6 days, correlating with ELMO1 expression (Fig. 3c). Recently, ELMO1 null mice have been described[36]. DCX$^+$ cells from mice lacking ELMO1 showed a significant reduction in phagocytic activity (2 day culture), compared with wild-type DCX$^+$ cells. After 6 days in culture, we could not detect any apoptotic targets inside *Elmo1*$^{-/-}$ DCX$^+$ cells (Fig. 3c). This indicated that ELMO1 is a key intracellular molecule regulating phagocytosis by DCX$^+$ cells. Notably, the differentiated GFAP$^+$ astrocytes from *Elmo1*$^{-/-}$ mice did not show a defect in phagocytosis when compared with astrocytes from wild-type mice (Supplementary Fig. S4).

When the SGZ and SVZ within the brains of *Elmo1*$^{-/-}$ mice were examined, there was a significant accumulation of TUNEL-positive nuclei (Fig. 3d and Supplementary Fig. S5a). This indicated an important role for ELMO1 in clearing apoptotic cells in the neurogenic niches. When the *Elmo1*$^{-/-}$ mice were treated long term with annexin V, there was a further increase in the accumulation of apoptotic debris (Fig. 3d), indicating that ELMO1-independent mechanisms for phagocytic clearance probably also exist.

We next examined adult neurogenesis in the *Elmo1*$^{-/-}$ mice. Wild-type and *Elmo1*$^{-/-}$ mice were injected with BrdU and their brains were examined for BrdU-containing DCX$^+$ cells after 7 days. Neuronal differentiation was substantially impaired in *Elmo1*$^{-/-}$ mice, compared with their wild-type counterparts (Fig. 4a), without affecting the total number of proliferating BrdU$^+$ cells. *Elmo1*$^{-/-}$ mice exhibited a significant reduction in the numbers of BrdU$^+$DCX$^+$ cells per hippocampus, reduced neuronal differentiation (BrdU$^+$DCX$^+$ of total BrdU$^+$) and lower counts of total DCX$^+$ cells per dentate gyrus (Fig. 4b).

Newly formed neurons from the SGZ migrate and integrate into the granular layer of the dentate gyrus and maintain its size in the adult animal. One of the indications for impaired adult neurogenesis is reduced width of the granular layer. *Elmo1*$^{-/-}$ mice exhibited a significantly thinner granular layer, indicative of impaired adult neurogenesis (Fig. 4c). As we did not observe a difference in the granular layer width and the numbers of DCX+ cells in neonatal *Elmo1*$^{-/-}$ versus wild-type mice, it seems that the reduced width of the granular layer was probably due to long-lasting impaired adult neurogenesis and not a developmental defect (Supplementary Fig. S5b). As glia can play a major role in debris clearance during development[25], either DCX$^+$ cells do not have a direct role in phagocytic clearance in the developing brain or less of a role when compared with glia, or perhaps clearance in the developing brain is ELMO1 independent.

Reduced DCX$^+$ cell numbers were also observed in the *Elmo1*$^{-/-}$ SVZ (Fig. 4d). Interestingly, the structure of DCX$^+$ cells in the SGZ revealed fewer DCX$^+$ cells in the *Elmo1*$^{-/-}$ hippocampus, with shorter processes and disorganized cell positioning in the SGZ (Fig. 4e). Long-term neurogenesis was also impaired without ELMO1, as determined by BrdU/NeuN labelling 28 days after BrdU injection, indicating an overall reduction in neuronal survival/maturation (Supplementary Fig. S5c).

To address whether the effect of ELMO1 was cell autonomous, we established neurosphere cultures with NPCs from the SVZ of adult wild-type and *Elmo1*$^{-/-}$ mice. There was no detectable difference in the general appearance of the neurospheres (Fig. 5a), or the number of neurospheres from the brains. The comparable sizes of the neurospheres (measured by the diameters of the neurospheres), the amplification and the self-renewal capacity within the neurospheres (indicative of 'stemness') indicated normal proliferative capacity

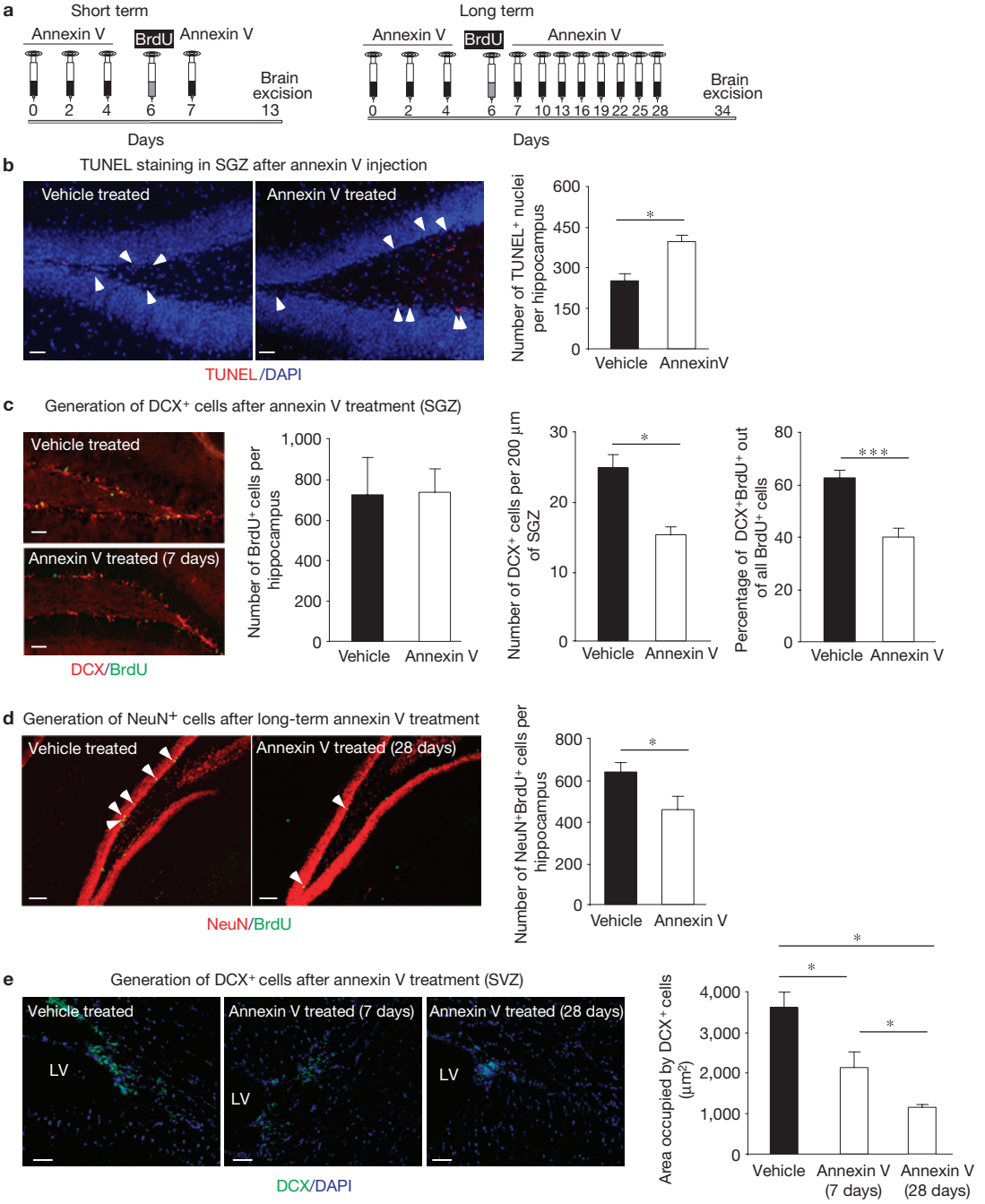

Figure 2 Inhibition of phagocytosis in the neurogenic niche *in vivo* impairs adult neurogenesis. (**a**) Schematic representation of short-term (7 days) and long-term (28 days) annexin V treatment to block apoptotic cell clearance, coupled with BrdU injection to monitor proliferating cells within the neurogenic zones. (**b**) Representative fluorescent microscopy images of accumulated apoptotic nuclei through TUNEL staining (indicated by white arrowheads) in the SGZ after short-term annexin V treatment. The bar graph represents a quantification of apoptotic (TUNEL-positive) nuclei (mean ± s.e.m.). Student's *t*-test statistical analysis was carried out for $n = 4$ mice in each group, with at least five slices analysed for each mouse ($^{*}P < 0.05$). Scale bars, 50 µm. (**c**) Representative fluorescent microscopy images of the SGZ from control and short-term annexin V-treated mice examined for DCX expression and BrdU incorporation. The bar graphs (means ± s.e.m.) represent quantifications of $BrdU^{+}$ cells (per hippocampus), DCX^{+} cells (per 200 µm of subgranular layer) and the fraction of $BrdU^{+}$ that were also DCX^{+} (indicative of neuronal differentiation; per hippocampus). Student's *t*-test statistical analysis was carried out for $n = 4$ mice in each group with at least ten slices analysed for each mouse ($^{*}P < 0.05$; $^{***}P < 0.001$). Scale bars, 50 µm. (**d**) Representative fluorescent microscopy images of control and long-term annexin V-treated brain slices examined for BrdU and NeuN immunoreactivity in the SGZ ($BrdU^{+}NeuN^{+}$ cells are indicated by white arrowheads). The bar graph represents quantification of $BrdU^{+}NeuN^{+}$ cells per hippocampus of vehicle- and annexin V-treated mice (mean ± s.e.m.). Student's *t*-test statistical analysis was carried out for $n = 7$ mice in each group with at least ten slices analysed for each mouse ($^{*}P < 0.05$). Scale bars, 50 µm. (**e**) Representative confocal microscopy images of the SVZ immunolabelled for DCX from control, short-term and long-term annexin V-treated mice (LV, lateral ventricle). The bar graph represents quantification of the areas occupied by DCX^{+} cells per field (mean ± s.e.m.). Student's *t*-test statistical analysis was carried out between the groups for $n = 5$ mice in each group with at least ten slices analysed for each mouse ($^{*}P < 0.05$). Scale bars, 50 µm.

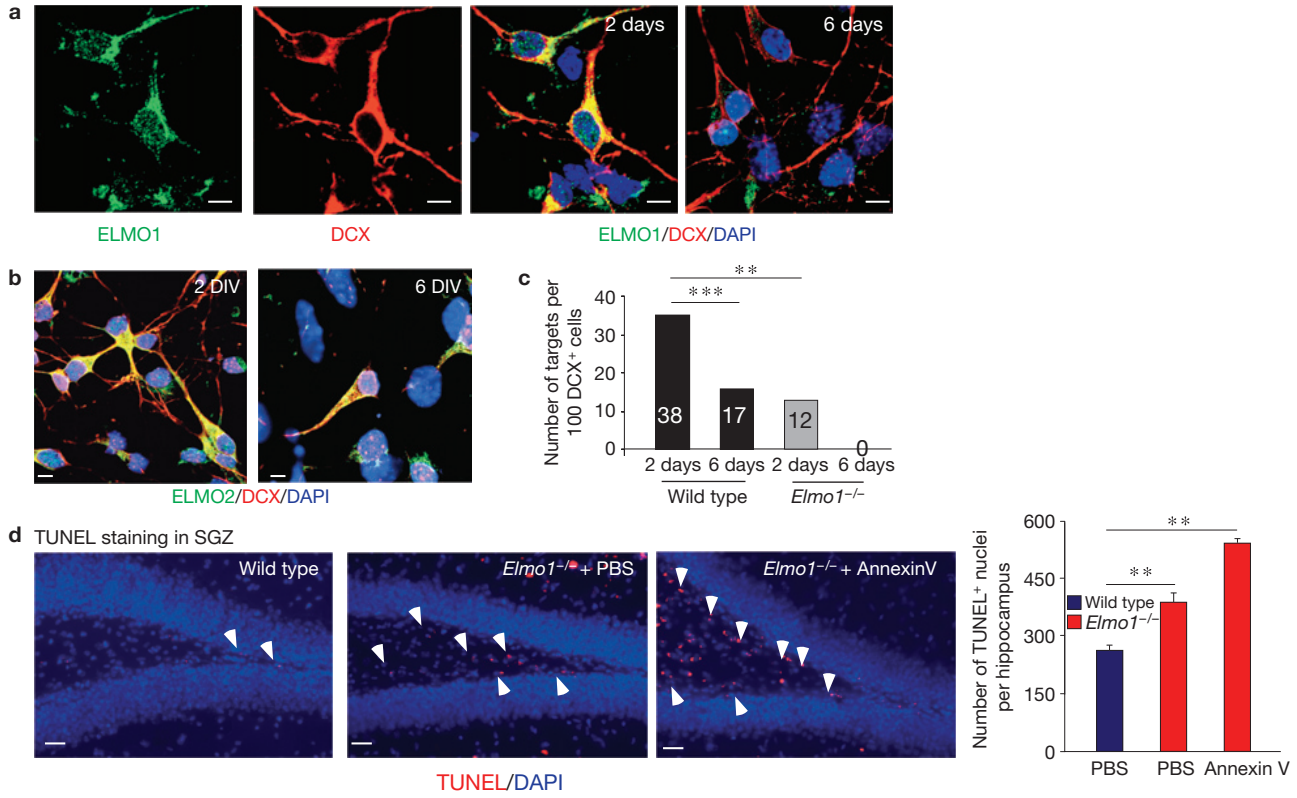

Figure 3 ELMO1-dependent phagocytosis of DCX$^+$ cells *in vitro*. (**a**) Representative images of primary hippocampal neuronal cultures grown for 2 or 6 days *in vitro* immunolabelled for DCX and ELMO1 (for $n > 30$ fields). Scale bars, 5 μm. (**b**) Primary hippocampal neuronal cultures grown for 2 or 6 days *in vitro* (DIV) were immunolabelled for DCX and ELMO2. Representative confocal microscopy images (for $n > 30$ fields) are shown. The expression level of ELMO2 was not altered under these conditions in the DCX$^+$ cells after 2 or 6 days in culture. Scale bars, 5 μm. (**c**) Cultures of neurons from **a** were fed with targets (carboxylate-modified beads) and assessed for engulfment. The bars represent quantifications of phagocytosed targets by primary DCX$^+$ cells from wild-type and *Elmo1*$^{-/-}$ mice after 2 or 6 days in culture. A one-way analysis of variance with a Newman–Keuls multiple comparison test was carried out for $n = 100$ DCX$^+$ cells per group ($^{**}P < 0.01$; $^{***}P < 0.001$). (**d**) Accumulation of apoptotic nuclei in PBS- or long-term annexin V-treated *Elmo1*$^{-/-}$ mice, compared with wild-type littermates, was examined by TUNEL immunolabelling (indicated by white arrowheads) of the SGZ. Representative images from wild-type and *Elmo1*$^{-/-}$ mice are shown. The bar graph represents a quantification of TUNEL-positive nuclei (mean ± s.e.m.). Student's *t*-test was carried out for $n = 5$ mice per group, with at least ten slices analysed for each mouse ($^{**}P < 0.01$). Scale bars, 50 μm.

of the progenitor constituents in the absence of ELMO1 (Fig. 5a). Neurospheres obtained from wild-type or *Elmo1*$^{-/-}$ mice did not basally show substantial apoptosis (by cleaved caspase 3 staining of cryosectioned neurospheres; Fig. 5b), perhaps owing to the nutrient-rich *in vitro* conditions. Importantly, there also was no difference in neuronal or astroglial differentiation *in vitro* between wild-type and *Elmo1*$^{-/-}$-derived NPCs (Fig. 5c). These data indicate that the impaired neuronal differentiation in *Elmo1*$^{-/-}$ mice *in vivo* probably resulted from extrinsic factors (such as impaired clearance of dying neurons) rather than intrinsic factors.

We then injected fluorescent PtdSer-containing liposomes into *Elmo1*$^{-/-}$ mice and examined the phagocytic ability of DCX$^+$ cells *in vivo*. When compared with wild-type littermates, the *Elmo1*$^{-/-}$ mice showed significantly fewer PtdSer liposomes phagocytosed by DCX$^+$ cells (>50% reduction). As the *Elmo1*$^{-/-}$ mice have fewer DCX$^+$ cells, we also compared the fluorescence of PtdSer within the normalized volumes of individual DCX$^+$ cells. Again, there was a substantial reduction in the phagocytosis mediated by DCX$^+$ cells *in vivo* (Fig. 5d; 24.5 ± 2% in wild-type mice, compared with 12 ± 1.5% in *Elmo1*$^{-/-}$ littermates; $P < 0.001$). These data support the notion that the defective phagocytic clearance and accumulation of apoptotic nuclei are the probable underlying cause for the impaired adult neurogenesis in *Elmo1*$^{-/-}$ mice.

Taken together, the data presented in this report provide several unexpected insights into the fundamentally important process of adult neurogenesis. First, these studies reveal DCX$^+$ cells as a critical population of phagocytes within the neurogenic niches of the adult brain. Second, these data identify the engulfment protein ELMO1 as an important molecule influencing adult neurogenesis through regulation of DCX$^+$ cell phagocytosis. Third, when phagocytic clearance was interfered with, either pharmacologically (via annexin V injection) or genetically (in the ELMO1 null mice), the relevance of phagocytic clearance of dying neurons for continued adult neurogenesis was revealed. Collectively, these findings indicate a paradigm wherein DCX$^+$ neuronal precursors are also phagocytes, and that such phagocytosis regulates neurogenesis in the adult brain. It is unclear whether all DCX$^+$ cells can engulf their dying brethren. Nevertheless, those DCX$^+$ cells that do engulf dying progenitors could differentiate and develop into neurons *in vitro*. Current technical challenges limit us to track the fate of phagocytic versus non-phagocytic DCX$^+$ cells *in vivo*. It is possible that phagocytosis of neighbouring dying progenitors could be advantageous for the phagocytic cell as an energy source.

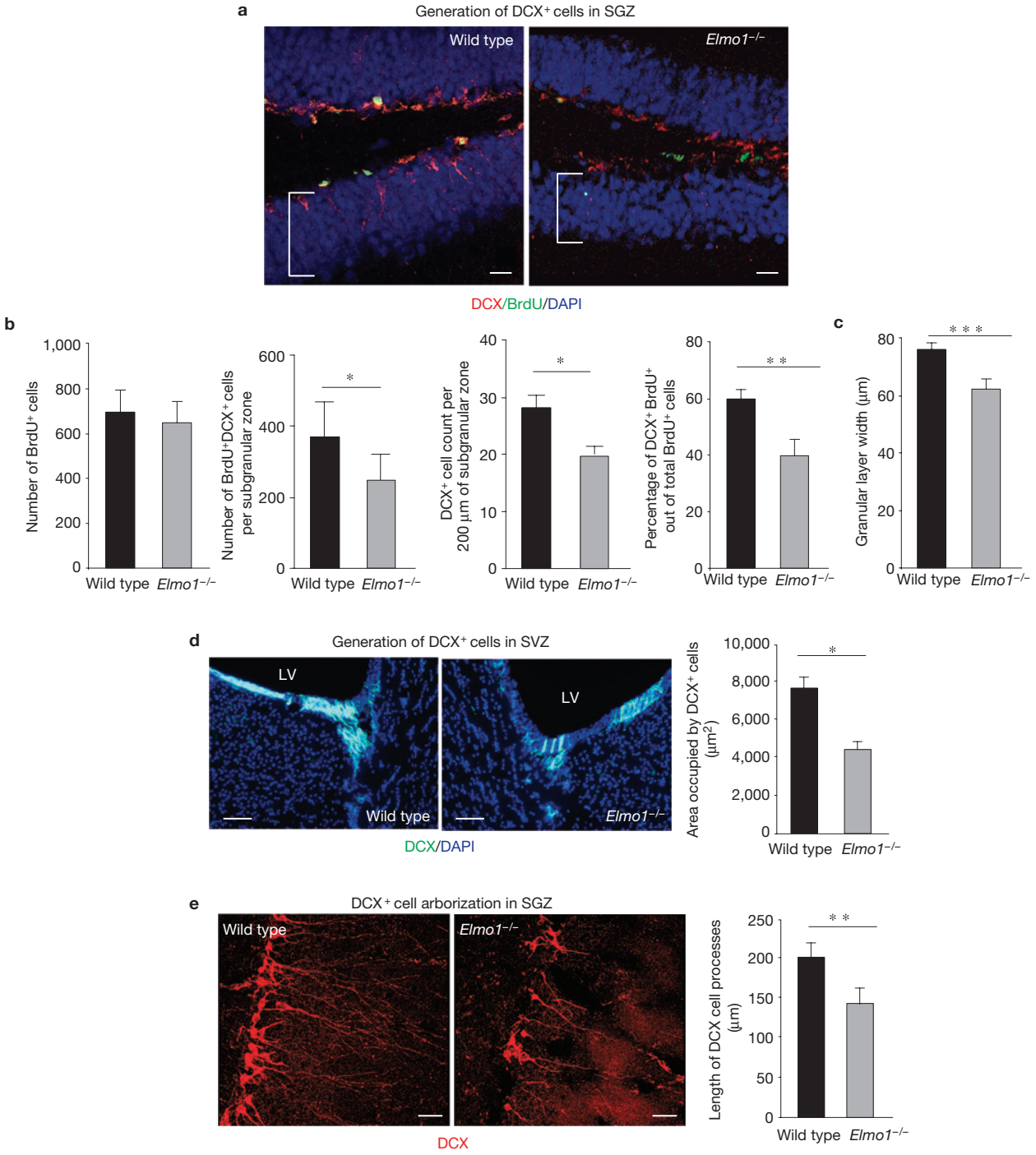

Figure 4 Effect of ELMO1-dependent phagocytosis of DCX$^+$ cells on neurogenesis *in vivo*. (**a**) Representative images of the SGZ from wild-type and *Elmo1*$^{-/-}$ mice examined for DCX and BrdU immunoreactivity 7 days after BrdU injection. The brackets indicate the width of the granular layer. Scale bars, 20 μm. (**b**) The bar graphs (means ± s.e.m.) represent the quantification of total numbers of BrdU$^+$ cells (proliferating cells), total numbers of all BrdU$^+$DCX$^+$ cells (neuronal progenitors), total numbers of DCX$^+$ cells per 200 μm of the SGZ (neuronal progenitors, alternative quantification) and percentages of DCX$^+$BrdU$^+$ out of all BrdU$^+$ cells (neuronal differentiation of proliferating cells) per hippocampus in wild-type and *Elmo1*$^{-/-}$ mice. Student's *t*-test statistical analysis was carried out for $n = 6$ mice in each group with at least ten slices analysed for each mouse ($^*P < 0.05$; $^{**}P < 0.01$). (**c**) Mean (±s.e.m.) width of a granular cell layer. Student's *t*-test was carried out for $n = 6$ mice per group with at least ten slices analysed for each mouse ($^{***}P < 0.001$). (**d**) Representative images of the SVZ immunolabelled for DCX from wild-type and *Elmo1*$^{-/-}$ mice (LV, lateral ventricle). The bar graph represents quantification of the areas occupied by DCX$^+$ cells per field (mean ± s.e.m.). Student's *t*-test statistical analysis was carried out between the groups for $n = 6$–8 mice in each group with at least ten slices analysed for each mouse ($^*P < 0.05$). Representative experiment out of three independently carried out ($n > 10$ fields analysed in each experiment). Scale bars, 50 μm. (**e**) High magnification of the SGZ immunolabelled for DCX$^+$ cells in wild-type and *Elmo1*$^{-/-}$ mice. The bar graph represents a quantification of dendritic arborization of DCX$^+$ cells in wild-type and *Elmo1*$^{-/-}$ mice (mean ± s.e.m.). Student's *t*-test statistical analysis was carried out for at least $n = 100$ DCX$^+$ cells in each group with at least $n = 5$ mice per group analysed ($^{**}P < 0.01$). Scale bars, 40 μm.

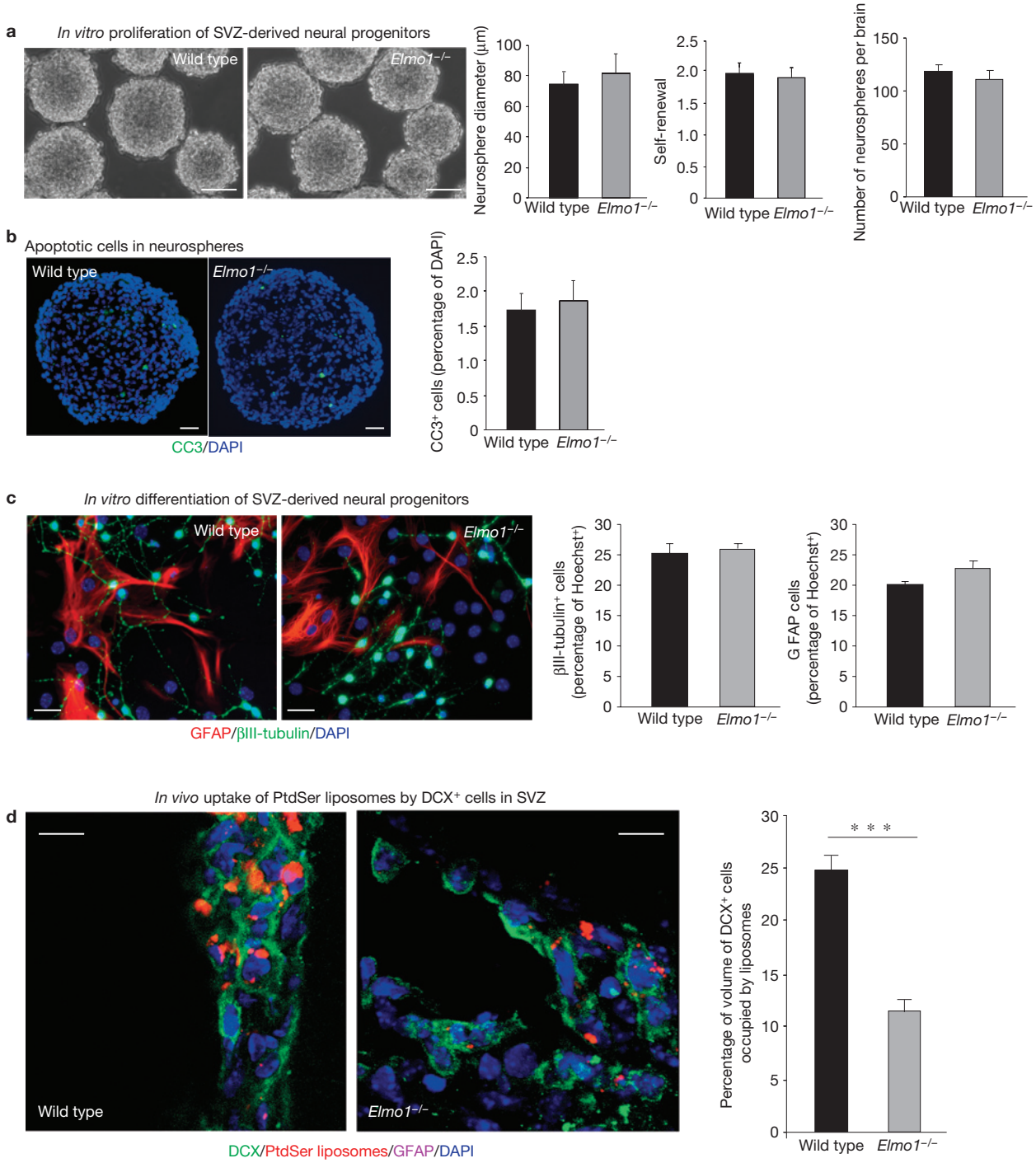

Figure 5 ELMO1 deficiency impairs phagocytic activity of DCX$^+$ cells *in vivo*. (**a**) Representative images of neurospheres from wild-type and *Elmo1*$^{-/-}$ mice. The bar graphs (means ± s.e.m.) show the diameter of neurospheres (indicates the ability of cells to grow and divide), the neurosphere self-renewal capacity (number of neurospheres divided by number of plated cells × 100) of the first-generation (P1) neurospheres and the initial number of neurospheres obtained from the adult brains of wild-type and *Elmo1*$^{-/-}$ mice ($n = 12$ mice in each group, with hundreds of neurospheres analysed). Scale bars, 50 μm. (**b**) Neurospheres established from NPCs obtained from *Elmo1*$^{-/-}$ or wild-type mice were cryosectioned and examined for apoptotic (cleaved caspase 3 (CC3)-positive) cells *in vitro*. Representative images (from $n > 5$ neurospheres) are shown. The bar graph indicates cleaved caspase 3-positive cells (percentage of all DAPI-positive cells) in the neurosphere (mean ± s.e.m.). Multiple fields for $n = 3$ neurospheres from each group were analysed. Scale bars, 20 μm. (**c**) Neurospheres established from NPCs obtained from *Elmo1*$^{-/-}$ or wild-type mice were examined for differentiation *in vitro*. Representative images of differentiated NPCs after 10 days in culture, immunolabelled for βIII-tubulin (neurons) and GFAP (astrocytes). The bar graphs (means ± s.e.m.) indicate neuronal differentiation (percentage of βIII-tubulin cells) and astrocyte differentiation (percentage of GFAP cells) from wild-type and *Elmo1*$^{-/-}$ neurospheres ($n = 10$ fields analysed in each experiment). Scale bars, 20 μm. (**d**) Wild-type and *Elmo1*$^{-/-}$ mice were injected with fluorescently labelled PtdSer liposomes and examined immunohistochemically for DCX$^+$ and GFAP$^+$ cells containing phagocytosed liposomes in the SVZ. Representative confocal micrographs are shown. The bar graph indicates a quantification of the volume of DCX cells with PtdSer liposomes in wild-type and *Elmo1*$^{-/-}$ mice (mean ± s.e.m.). Student's *t*-test statistical analysis was carried out for $n = 4$ mice in each group with at least five slices analysed for each mouse (*** $P < 0.001$). Scale bars, 10 μm.

However, precisely how the phagocytosis is advantageous for neuronal differentiation, maturation and survival *in vivo* remains to be defined.

DCX$^+$ neuronal progenitor cells constitute an essential group of cells that differentiate into mature neurons during neurogenesis. Microglia have been recently shown to have close contact with dying NPCs in the SGZ and by inference were thought to mediate phagocytosis[37]. When we attempted to deplete ELMO1 in microglial cells (LysM-Cre mice crossed with *Elmo1*$^{flox/flox}$ mice), phagocytic clearance seemed normal without affecting adult neurogenesis (Supplementary Fig. S6). However, a caveat was that using the LysM-Cre we could only achieve partial deletion efficiency for the *Elmo1* loci within the microglia. Interestingly, ELMO1 deficiency does not seem to affect the phagocytic capacity of myeloid cells[36]. Thus, whereas these data do not rule out a role for microglial cells in phagocytic clearance during adult neurogenesis, the impaired neurogenesis seen in *Elmo1*$^{-/-}$ mice is probably primarily due to the defective engulfment by DCX$^+$ neuronal progenitor cells. Intriguingly, the survival of newborn neurons is improved under conditions that promote brain activity, such as hippocampus-dependent cognitive tasks, or enriched environment[7,38,39]. Identifying phagocytosis as an unexpected further property of neuronal cells may have a significant impact on further understanding adult neurogenesis in physiological and pathological conditions. □

METHODS

Methods and any associated references are available in the online version of the paper at http://www.nature.com/naturecellbiology

Note: Supplementary Information is available on the Nature Cell Biology website

ACKNOWLEDGEMENTS

We thank S. Smith for editing the original version of the manuscript and S. Zeitlin for comments. We also thank the members of the Kipnis and Ravichandran laboratories for discussions at many stages of conducting the work and the preparation of the manuscript. This work was supported in part by an award from the National Institute of General Medical Sciences (GM55761) to K.S.R. and in part by an award from the National Institute on Aging (R01AG034113) to J.K. K.S.R. is a Bill Benter Senior Fellow of the American Asthma Foundation.

AUTHOR CONTRIBUTIONS

Z.L. participated in the experimental design, carried out most of the experiments, analysed the data and participated in manuscript preparation; M.R.E. assisted with phagocytic assays and participated in experimental design; Y.C. assisted with immunofluorescent experiments; J.T.W. assisted with intracranial injections; A.L.K. supplied all the liposomes used in this study; K.S.R. helped with design of experiments and prepared the manuscript; J.K. designed the experiments, assisted with data analysis and prepared the manuscript.

COMPETING FINANCIAL INTERESTS

The authors declare no competing financial interests.

Published online at http://www.nature.com/naturecellbiology
Reprints and permissions information is available online at http://www.nature.com/reprints

1. van Praag, H. *et al.* Functional neurogenesis in the adult hippocampus. *Nature* **415,** 1030–1034 (2002).
2. Eriksson, P. S. *et al.* Neurogenesis in the adult human hippocampus. *Nat. Med.* **4,** 1313–1317 (1998).
3. Zhao, C., Deng, W. & Gage, F. H. Mechanisms and functional implications of adult neurogenesis. *Cell* **132,** 645–660 (2008).
4. Kornack, D. R. & Rakic, P. Cell proliferation without neurogenesis in adult primate neocortex. *Science* **294,** 2127–2130 (2001).
5. Rakic, P. Adult neurogenesis in mammals: an identity crisis. *J. Neurosci.* **22,** 614–618 (2002).
6. Rakic, P. Neurogenesis in adult primate neocortex: an evaluation of the evidence. *Nat. Rev. Neurosci.* **3,** 65–71 (2002).
7. Kempermann, G., Kuhn, H. G. & Gage, F. H. More hippocampal neurons in adult mice living in an enriched environment. *Nature* **386,** 493–495 (1997).
8. Ziv, Y. *et al.* Immune cells contribute to the maintenance of neurogenesis and spatial learning abilities in adulthood. *Nat. Neurosci.* **9,** 268–275 (2006).
9. Leuner, B. *et al.* Learning enhances the survival of new neurons beyond the time when the hippocampus is required for memory. *J. Neurosci.* **24,** 7477–7481 (2004).
10. Gould, E., Beylin, A., Tanapat, P., Reeves, A. & Shors, T. J. Learning enhances adult neurogenesis in the hippocampal formation. *Nat. Neurosci.* **2,** 260–265 (1999).
11. Wolf, S. A. *et al.* CD4-positive T lymphocytes provide a neuroimmunological link in the control of adult hippocampal neurogenesis. *J. Immunol.* **182,** 3979–3984 (2009).
12. Kempermann, G., Gast, D., Kronenberg, G., Yamaguchi, M. & Gage, F. H. Early determination and long-term persistence of adult-generated new neurons in the hippocampus of mice. *Development* **130,** 391–399 (2003).
13. Kronenberg, G. *et al.* Subpopulations of proliferating cells of the adult hippocampus respond differently to physiologic neurogenic stimuli. *J. Comp. Neurol.* **467,** 455–463 (2003).
14. Kempermann, G., Jessberger, S., Steiner, B. & Kronenberg, G. Milestones of neuronal development in the adult hippocampus. *Trends Neurosci.* **27,** 447–452 (2004).
15. Ma, D. K., Kim, W. R., Ming, G. L. & Song, H. Activity-dependent extrinsic regulation of adult olfactory bulb and hippocampal neurogenesis. *Ann. N Y Acad. Sci.* **1170,** 664–673 (2009).
16. Mandyam, C. D., Harburg, G. C. & Eisch, A. J. Determination of key aspects of precursor cell proliferation, cell cycle length and kinetics in the adult mouse subgranular zone. *Neuroscience* **146,** 108–122 (2007).
17. Gregory, C. D. & Pound, J. D. Cell death in the neighbourhood: direct microenvironmental effects of apoptosis in normal and neoplastic tissues. *J. Pathol.* **223,** 177–194 (2011).
18. Nagata, S., Hanayama, R. & Kawane, K. Autoimmunity and the clearance of dead cells. *Cell* **140,** 619–630 (2010).
19. Elliott, M. R. & Ravichandran, K. S. Clearance of apoptotic cells: implications in health and disease. *J. Cell Biol.* **189,** 1059–1070 (2010).
20. Doetsch, F., Caille, I., Lim, D. A., Garcia-Verdugo, J. M. & Alvarez-Buylla, A. Subventricular zone astrocytes are neural stem cells in the adult mammalian brain. *Cell* **97,** 703–716 (1999).
21. Conover, J. C. *et al.* Disruption of Eph/ephrin signaling affects migration and proliferation in the adult subventricular zone. *Nat. Neurosci.* **3,** 1091–1097 (2000).
22. Song, H. J., Stevens, C. F. & Gage, F. H. Neural stem cells from adult hippocampus develop essential properties of functional CNS neurons. *Nat. Neurosci.* **5,** 438–445 (2002).
23. Song, H., Stevens, C. F. & Gage, F. H. Astroglia induce neurogenesis from adult neural stem cells. *Nature* **417,** 39–44 (2002).
24. McFarland, K. N., Wilkes, S. R., Koss, S. E., Ravichandran, K. S. & Mandell, J. W. Neural-specific inactivation of ShcA results in increased embryonic neural progenitor apoptosis and microencephaly. *J. Neurosci.* **26,** 7885–7897 (2006).
25. Wu, H. H. *et al.* Glial precursors clear sensory neuron corpses during development via Jedi-1, an engulfment receptor. *Nat. Neurosci.* **12,** 1534–1541 (2009).
26. Ziegenfuss, J. S. *et al.* Draper-dependent glial phagocytic activity is mediated by Src and Syk family kinase signalling. *Nature* **453,** 935–939 (2008).
27. MacDonald, J. M. *et al.* The *Drosophila* cell corpse engulfment receptor Draper mediates glial clearance of severed axons. *Neuron* **50,** 869–881 (2006).
28. D'Arceuil, H. *et al.* 99mTc annexin V imaging of neonatal hypoxic brain injury. *Stroke* **31,** 2692–2700 (2000).
29. Zhang, X. *et al.* A minimally invasive, translational biomarker of ketamine-induced neuronal death in rats: microPET Imaging using 18F-annexin V. *Toxicol. Sci.* **111,** 355–361 (2009).
30. Maeda, Y., Shiratsuchi, A., Namiki, M. & Nakanishi, Y. Inhibition of sperm production in mice by annexin V microinjected into seminiferous tubules: possible etiology of phagocytic clearance of apoptotic spermatogenic cells and male infertility. *Cell Death Differ.* **9,** 742–749 (2002).
31. Reed-Geaghan, E. G., Savage, J. C., Hise, A. G. & Landreth, G. E. CD14 and toll-like receptors 2 and 4 are required for fibrillar Aβ-stimulated microglial activation. *J. Neurosci.* **29,** 11982–11992 (2009).
32. Koenigsknecht-Talboo, J. & Landreth, G. E. Microglial phagocytosis induced by fibrillar β-amyloid and IgGs are differentially regulated by proinflammatory cytokines. *J. Neurosci.* **25,** 8240–8249 (2005).
33. Koenigsknecht, J. & Landreth, G. Microglial phagocytosis of fibrillar β-amyloid through a β1 integrin-dependent mechanism. *J. Neurosci.* **24,** 9838–9846 (2004).
34. Park, D. *et al.* BAI1 is an engulfment receptor for apoptotic cells upstream of the ELMO/Dock180/Rac module. *Nature* **450,** 430–434 (2007).
35. Gumienny, T. L. *et al.* CED-12/ELMO, a novel member of the CrkII/Dock180/Rac pathway, is required for phagocytosis and cell migration. *Cell* **107,** 27–41 (2001).
36. Elliott, M. R. *et al.* Unexpected requirement for ELMO1 in clearance of apoptotic germ cells *in vivo*. *Nature* **467,** 333–337 (2010).
37. Sierra, A. *et al.* Microglia shape adult hippocampal neurogenesis through apoptosis-coupled phagocytosis. *Cell Stem Cell* **7,** 483–495 (2010).
38. Brown, J. *et al.* Enriched environment and physical activity stimulate hippocampal but not olfactory bulb neurogenesis. *Eur. J. Neurosci.* **17,** 2042–2046 (2003).
39. Kempermann, G., Brandon, E. P. & Gage, F. H. Environmental stimulation of 129/SvJ mice causes increased cell proliferation and neurogenesis in the adult dentate gyrus. *Curr. Biol.* **8,** 939–942 (1998).

METHODS

Animals. *Elmo1*$^{-/-}$ mice and their littermates were bred in our facilities and C57Bl/6J mice (used for Annexin V injection studies) were purchased from the Jackson laboratories. Animals were housed in identical light- and temperature-controlled rooms and age-matched mice at ages 8–12 weeks were used throughout the study (except for Supplementary Fig. S2a, where 5-week-old mice were used, and this is indicated in the figure legend). All experiments were conducted under University of Virginia Animal Care and Use Committee-approved protocols. Male mice were used in the experiments in this manuscript.

Neurosphere culture. Neurospheres were generated from the SVZ of young adult mice and cultured under clonal conditions, according to previously published procedures[40]. Briefly, for each culture, the entire SVZ region was dissected from sagittally cut brains and incubated in DMEM containing 20 U ml^{-1} papain (Worthington), 1 mM *N*-acetyl-L-cysteine (NAC; Sigma) and 2 U ml^{-1} RQ1 DNase (Promega) for 1 h at 37 °C. Dissociated cells were plated in 24-well plates at a density of 2.6×10^3 cells cm^{-2} (5×10^3 cells in 0.5 ml per well) in high-glucose DMEM containing N2 (Invitrogen), B-27 (StemCell Technologies), 1 mM NAC, 1 mM sodium pyruvate, 2 mM L-glutamine, 20 ng ml^{-1} epidermal growth factor and 20 ng ml^{-1} basic fibroblast growth factor (both murine growth factors were from PeproTech). The total number of neurospheres at passage 0 (P0) was determined at 7 DIV by counting all neurospheres generated from each mouse brain. In subsequent passages, the total number of neurospheres was determined by counting all neurospheres generated in a 24-well dish seeded at 5×10^3 cells per well and extrapolating for the total number of dissociated cells. Self-renewal was determined as the number of secondary neurospheres/number of seeded cells × 100 (that is, how many early precursors capable of generating a 'daughter' neurosphere were contained in each 'mother' neurosphere). Amplification was calculated as the number of viable cells from dissociated neurospheres/number of seeded cells. The number of viable cells was determined in samples of SVZ- or neurosphere-dissociated cells by trypan blue exclusion. Neurosphere diameter (>40 μm) was measured in phase-contrast pictures of individual neurospheres using QCapture Pro 6.0 software (QImaging). For the cell differentiation study, neurospheres were dissociated in papain or accutase (Invitrogen) solution. Dissociated single cells were seeded on coverslips coated with poly-L-lysine. Cells were kept in differentiation medium for either 7 or 14 days, with half of the medium changed every other day.

NPC differentiation. Dissociated NPCs were plated at 8×10^3 cells cm^{-2} on poly-L-lysine-coated coverslips and maintained in the differentiation medium (high-glucose DMEM containing N2, B-27, 1 mM NAC, 1 mM sodium pyruvate, 2 mM L-glutamine and 1% fetal bovine serum) for 7 days. Half of the medium was replaced with fresh medium every other day. For immunofluorescent staining, the following primary antibodies were used on 4% paraformaldehyde-fixed cells: goat anti-DCX (1:200, Santa Cruz) and rabbit anti-GFAP (1:500, Millipore). Fluorescently labelled cells were visualized and imaged on a confocal microscope (Zeiss LSM510; Carl Zeiss).

NPC ultraviolet-irradiation treatment and NPC injection. Dissociated NPCs were treated with ultraviolet light for 15 min. NPCs were then stained with 5(6)-TAMRA, SE (Invitrogen) and thoroughly washed with cold PBS before they were used for either incubation with cell culture or intracranial injection. For intracranial injection, 2 μl of a 5 million cells ml^{-1} suspension was injected into the lateral ventricles of mice using a stereotaxic injector (Stoelting).

BrdU treatment. BrdU (Sigma) was dissolved in 0.9% saline at a concentration of 5 mg ml^{-1}. To label proliferating cells in the brain, mice received two intraperitoneal injections of BrdU (50 mg kg^{-1}) 2 h apart. For examination of progenitor proliferation mice were killed 24 h after the second injection, whereas for examination of progenitor differentiation mice were killed 7 days after BrdU injection. For examination of neuronal survival (NeuN$^+$BrdU$^+$ cells in the granular layer), animals were injected with a double dose of BrdU and killed 28 days after injection. Mice were perfused with PBS for 3 min and then with 4% paraformaldehyde (PFA) in pH 7.2 PBS for 5 min. Brains were excised and postfixed in 4% PFA for 72 h at 4 °C, then in 30% sucrose for at least 2 days. Brains were frozen in 2-methylbutane Chromasolv with dry ice, and stored at −80 °C before coronal cryostat sections (40 μm thick) were obtained. Six sequential slices were placed into each well of a 24-well plate containing 0.02% sodium azide in PBS and stored at 4 °C. To quantify proliferating progenitor cells, every sixth section (40 μm thick) of the brain containing hippocampus or lateral ventricles was selected and immunolabelled with BrdU (rat anti-BrdU, 1:300; Abcam), DCX (goat anti-DCX, 1:200; Santa Cruz) or NeuN (1:300; Millipore) antibodies. Total numbers of positive cells in all slices per animal were multiplied by six to estimate the number of cells per hippocampus or lateral ventricles.

Immunofluorescence. For BrdU labelling on coronal free-floating sections, the sections were permeabilized with 0.5% Triton X-100 in PBS for 20 min, and then treated with 0.3% H_2O_2 to block endogenous peroxidases, denatured in 2 N HCl for 15 min, and rinsed twice in 0.1 M (pH 8.5) borate buffer. Sections were placed in 10% normal chicken serum in PBS for 1 h, then incubated with primary antibody rat anti-BrdU (1:300; Abcam) overnight at 4 °C. For DCX, GFAP and NeuN labelling, brain slices were permeabilized with 0.5% Triton X-100 in PBS for 1 h. Following blocking, the slices were incubated with goat anti-DCX (1:300; Santa Cruz), rabbit anti-GFAP (1:800, Millipore) or mouse anti-NeuN (1:300; Millipore) antibodies, and fluorescent-dye-conjugated secondary antibodies were used to label the cells. To detect ELMO1 and DCX in cultured hippocampus neurons, rabbit anti-ELMO1 (1:100, Sigma) and goat anti-DCX (1:300, Santa Cruz) were used to label cultured neurons on coverslips.

TUNEL assay. An *in situ* cell-death detection kit (catalogue no 11684795001; Roche) was used to detect cell apoptosis in the mouse brain, according to the manufacturer's instructions.

Liposome preparation and injection. Liposomes were prepared by a classical Bangham technique; multilamellar vesicles were chosen for the study to maximize the fluorescent-dye load per particle without significant self-quenching. Briefly, dioleoyl phosphatidylcholine (Avanti Polar Lipids) and cholesterol (Sigma) were mixed in chloroform at 1:1 molar ratio, and DiIC18(3) dye (Invitrogen) was added; this dye has two stearyl residues attached to the fluorochrome, so it is tightly attached to liposome membrane and is not exchangeable. To the experimental sample but not to control, PtdSer (Avanti) was added at 1:10 PS:PC mass ratio. After chloroform removal by rotary evaporation and argon-gas flush, vacuum desiccation was applied to remove traces of organic solvent. After removal of the solvent had been completed, normal saline was added to the lipid film, and the sample was subjected to hydration under vortexing. Resulting liposomes were quite large: at normal gravity, sedimentation was observed during storage.

***In vitro* and *in vivo* phagocytosis assay.** To determine whether DCX$^+$ cells could engulf apoptotic cells or simplified targets, NPCs were differentiated for 48 h and carboxylate-modified 3 μm beads (simplified apoptotic targets) were fed to the cells for 3 h before thoroughly washing and then fixing the cells with 4% PFA. Cells were immunolabelled with anti-DCX antibody and Alexa Fluor 488 phalloidin (1:50, Invitrogen). Beads with a clear surrounding actin ring were counted as engulfed. Alternatively, dissociated single NPCs were exposed to ultraviolet light for 10 min before their feeding to growing cultures of differentiating NPCs for 4 h, washing and fixing in 4% PFA. To assess cells' engulfment capacity *ex vivo*, 1 μl of PtdSer- or PtdCho-coated liposomes (diameter 2–6 μm) were stereotaxically injected intracranially into the SVZ. Mice were killed 12 h after the injection and perfused with PBS. Brains were removed and fixed in 4% PFA. Floating sections (40 μm) were analysed for phagocytic cells as described above (every sixth slice was labelled and counted throughout the entire neurogenic niche). All of the images analysed and provided in the manuscript were taken approximately within the range of 200 μm of the injection site (liposomes were well diffused, whereas the progenitor cells did not diffuse equally well, which presumably results in the lower numbers of phagocytic DCX$^+$ when counting progenitor-engulfing DCX$^+$ cells as compared with liposome-engulfing DCX$^+$ cells *in vivo*).

Annexin V intravenous injection. To address the role of phagocytic cell clearance in adult neurogenesis (Fig. 2), annexin V (BioVision) was intravenously injected at a dose of 5 μg per 100 μl using the scheme shown in Fig. 2a. To assess the effect of annexin V on DCX$^+$ cell phagocytic activity *in vivo*, annexin V was injected three times before BrdU administration, followed by a further two injections (5 μg per 100 μl intravenously every 2 h).

Statistical tests. In this study we employed Student's *t*-test for comparison between two groups and analysis of variance with the Newman-Keuls test for multiple-group comparison.

40. Lu, Z. & Kipnis, J. Thrombospondin 1—a key astrocyte-derived neurogenic factor. *FASEB J.* **24,** 1925–1934 (2010).

nature cell biology

DOI: 10.1038/ncb2299

a

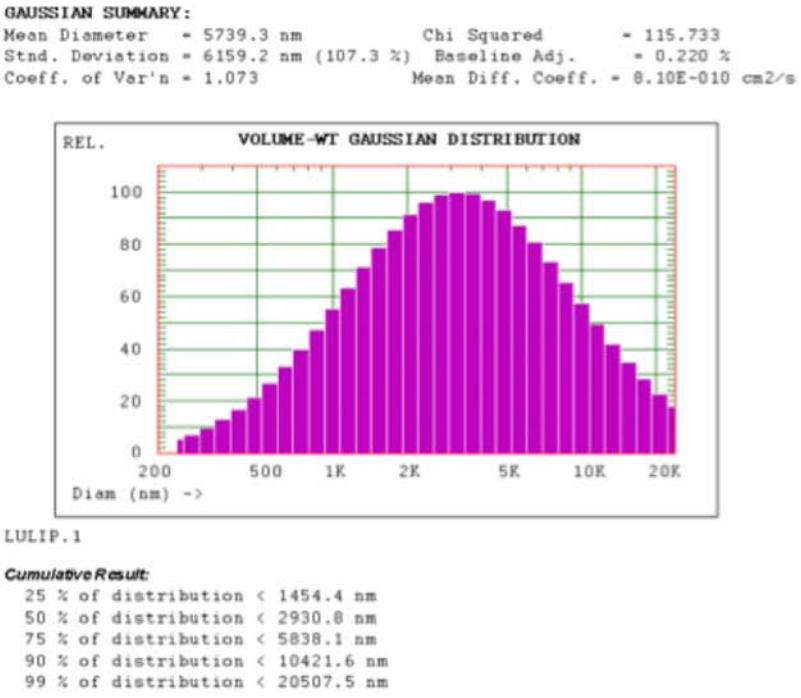

b

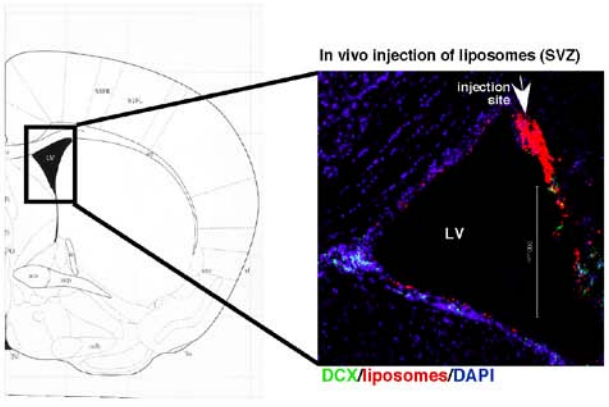

c

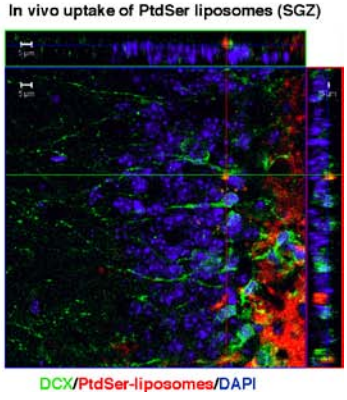

Figure S1 Physical properties of the liposomes and their intracranial injection. **(a)** Gaussian volume distribution data for the liposome preparation was obtained using dynamic laser light scattering performed with a Nicomp 370 instrument (Accucomp, Santa Barbara, CA). The median size of the particle was 5.7 μm with > 75% of the particles being over 1.5 μm in diameter. Briefly, the methodology used was as follows: an aliquot of liposomes was dispersed in normal saline and placed in a round cuvette and the measurement performed at room temperature. Particle counting using Coulter principle was performed on a Multisizer 3 instrument (Beckman-Coulter, Hialeah, FL). The instrument was calibrated with standard polystyrene latex beads and was operated in volumetric mode, with 0.5 ml sample taken through a 50 μm orifice. Volume distribution data is presented. **(b)** (left) Coronal image from the Mouse Brain Atlas indicating the location of the lateral ventricles and the injection site of liposomes. (right) The phagocytic activity of DCX cells near the injection site was examined in the area within approximately 200 μm (as indicated). **(c)** Wild type mice intracranially injected with fluorescently labeled phosphatydilserine (PtdSer) liposomes were examined immunohistochemically in the subgranular zone (SGZ) for DCX^+ cells with phagocytosed liposomes. Representative confocal micrograph is shown. Data from one representative experiment out of 3 independent experiments is shown (n > 10 fields analyzed in each experiment; n = 4 mice/group). Scale bar = 5 μm.

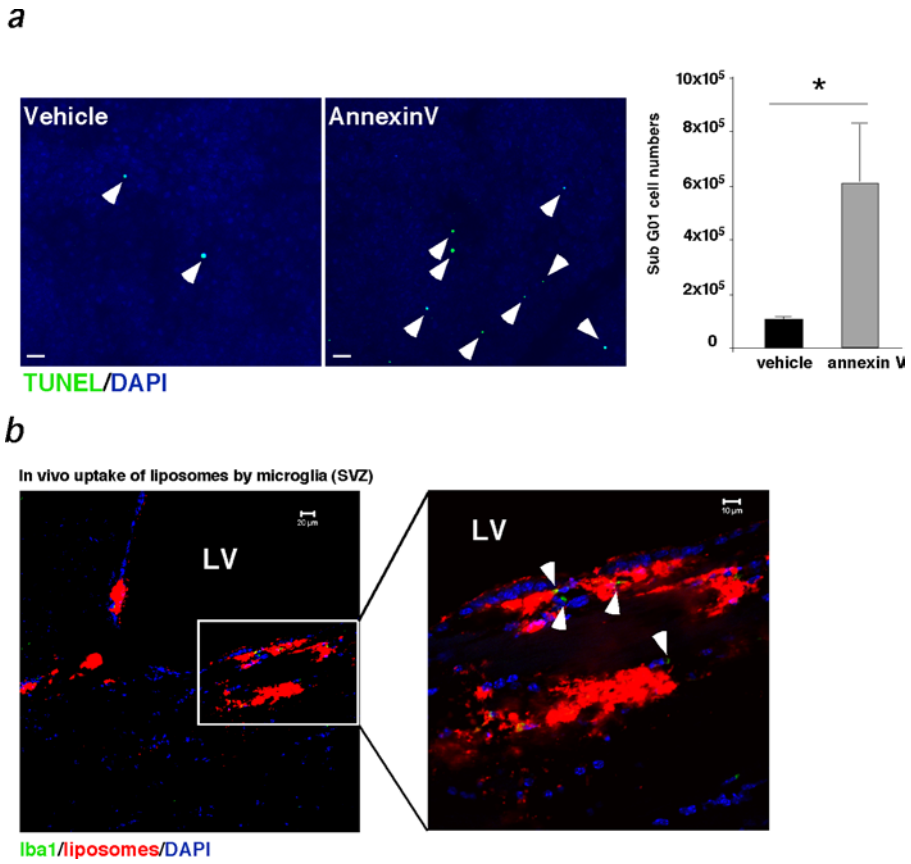

Figure S2 Accumulation of apoptotic debris in the thymus and microglia activity in the brain in annexinV-treated mice. **(a)** B6 mice (aged 5weeks) were given two i.v. injections of 20ug annexin V or vehicle at t=0 and t=3h. At t=6h, mice were euthanized and thymus collected for either histology or prepared for analysis flow cytometry. The rationale was that normal thymus has a high turnover of immature thymocytes that undergo apoptosis and that blocking their uptake via annexin V (which masks PtdSer dependent engulfment) would lead to increased number of uncleared corpses. Representative fluorescent images of accumulated apoptotic nuclei via TUNEL staining (indicated by arrowheads) in the thymus after short-term annexin V (or vehicle) treatment. Scale bar = 20 μm. Bar graph represents a quantification of apoptotic (sub G0) thymocytes as analyzed by flow cytometry (average ± s.e.m.). Student's t-test statistical analysis was performed from n = 3 mice in each group (*, $p < 0.05$). **(b)** Wild type mice intracranially injected with fluorescently labeled liposomes were examined immunohistochemically in the subventricular zone (SVZ) for $Iba1^+$ cells. Only few Iba1+ cells with were determined along the ventricular walls (indicated by arrow heads). Representative confocal micrographs (of different magnifications) are shown. Representative experiment out of 3 independently performed (n > 20 fields analyzed in each experiment; n = 4 mice/group). Scale bar = 10 μm.

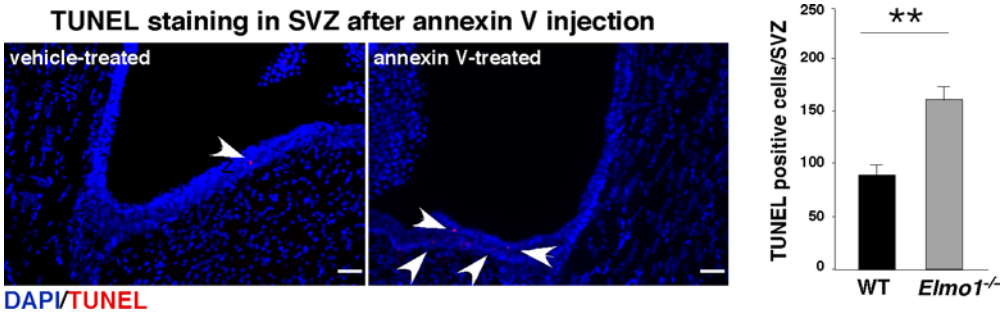

Figure S3 Accumulation of apoptotic debris in SVZ in annexinV-treated mice. Accumulation of apoptotic nuclei (indicated by arrowheads) in the subventricular zone (SVZ) was determined via TUNEL staining after short-term annexin V treatment. Representative images are shown (n = 3 mice in each group with at least 8 slices analyzed for each mouse). Quantification of TUNEL positive cells per subventricular zone (average ± s.e.m.) is an extrapolation based on 12 brain slices from each mouse (approx. 200μm apart) with n = 4 mice/group. Scale bar = 50 μm.

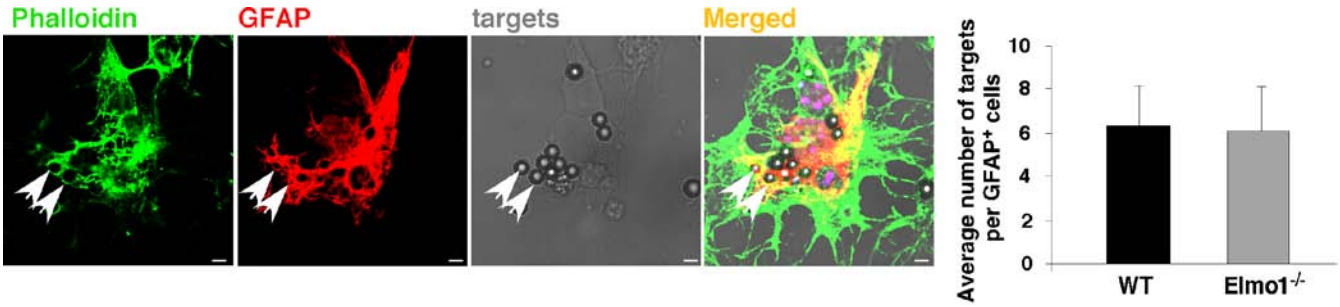

Figure S4 Elmo1 in astrocyte phagocytic activity. Representative images of astrocytes from wild type and *Elmo1*$^{-/-}$ mice engulfing simplified targets (negatively charged carboxyl-modified beads). Bar graphs represents quantification of total phagocytosed targets by astrocytes from wild type and *Elmo1*$^{-/-}$ mice (average ± s.e.m.). Scale bar = 3 μm. Representative experiment out of 3 independently performed (n > 10 fields analyzed in each experiment). Scale bar = 10 μm.

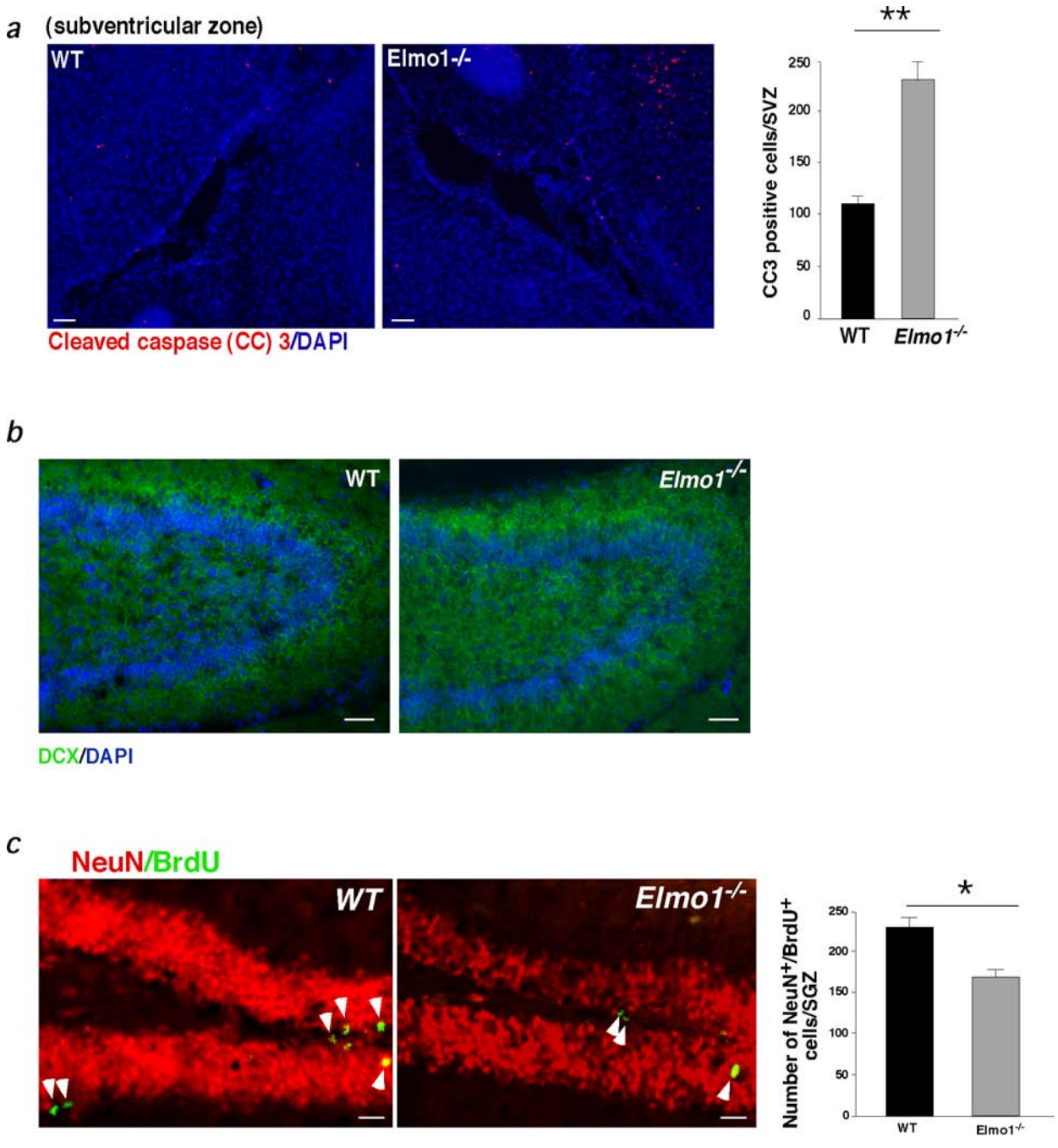

Figure S5 Roles of ELMO1 in neurogenesis. **(a)** Representative images of cleaved caspases 3 labeling in the SVZ from wild type and *Elmo1*$^{-/-}$ mice. Bar graph represents quantification of CC3 positive cells per subventricular zone, which is an extrapolation based on 12 brain slices from each mouse (approx. 200μm apart) with n = 4 mice/group (average ± s.e.m.). Scale bar = 50 μm. **(b)** No significant difference in general DCX fluorescence or in gross anatomy was evident between neonatal wild type and *Elmo1*$^{-/-}$ mice (n = 4 mice/group). Scale bar = 20 μm. **(c)** Representative images from *Elmo1*$^{-/-}$ mice labeled for NeuN (red) and BrdU (green) 30 days after BrdU injection. Bar graph represents quantification of NeuN^{+}BrdU^{+} cells in SGZ of wild type and *Elmo1*$^{-/-}$ mice (average ± s.e.m.). Student's t-test statistical analysis was performed from n = 6 mice in each group with at least 10 slices analyzed for each mouse (*, $p < 0.05$). Scale bar = 20 μm.

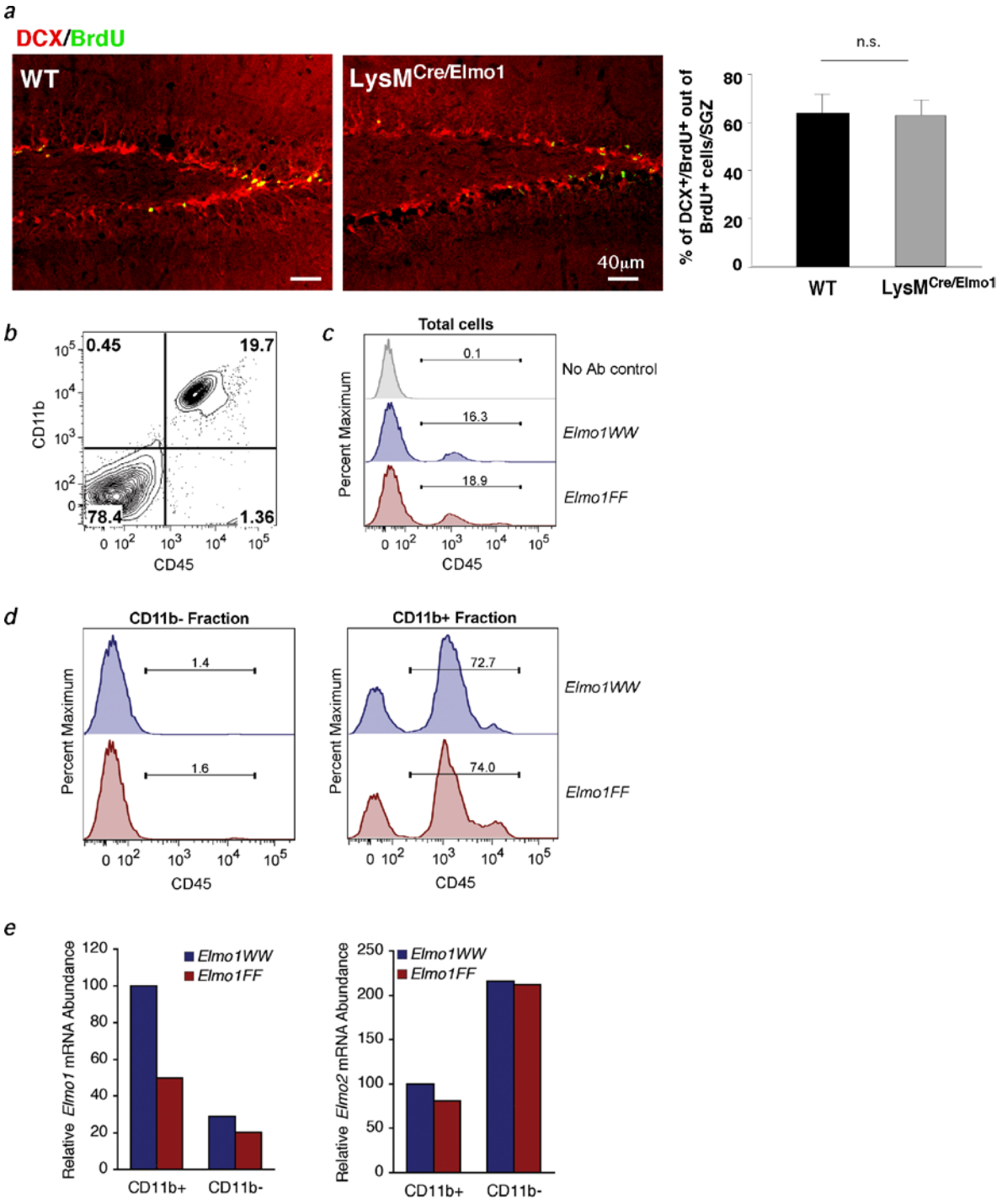

Figure S6 LysM$^{Cre/Elmo1}$ mice do not exhibit any apparent impairment in adult neurogenesis. **(a)** Representative confocal images from LysM$^{Cre/Elmo1}$ mice labeled for DCX (red) and BrdU (green) 7 days after BrdU injection. Bar graphs represent percentage of neuronal differentiation of all BrdU positive cells seven days after BrdU injection in wild type and LysM$^{Cre/Elmo1}$ mice (average ± s.e.m.). Representative experiment out of 3 independently performed (n = 5 mice/group). Scale bar = 10 μm. Scale bar = 40 μm. **(b-e)** Total cells were isolated from the brains of adult *LysM*-Cre+ mice carrying wild-type (*WW*) or floxed (*FF*) *Elmo1* alleles and enriched by anti-CD11b column separation. **(b)** Non-enriched (total) cells from wild-type mice were stained with antibodies to CD45 and CD11b and analyzed by flow cytometry. Note that >90% of CD45+ cells are also CD11b^{+}. (**c-d**) The enrichment of the populations obtained from the column separation was determined by anti-CD45 staining of the non-enriched (**c**), CD11b-depleted (**d,** left) and CD11b-enriched (**d**, right) fractions from *Elmo1WW* and *Elmo1FF* mice. Non-viable cells were excluded from the analysis by propidium iodide staining. (**e**) Relative mRNA levels of *Elmo1* (left) and *Elmo2* (right) in *Elmo1WW* and *Elmo1FF* mice were determined in the indicated cell fractions by quantitative PCR analysis. In **c-e**, total cells were pooled from two littermates per genotype prior to analysis and column enrichment.